GEODESIC PROPERTIES OF A GENERALIZED WASSERSTEIN EMBEDDING FOR TIME SERIES ANALYSIS

Shiying Li*
Department of Biomedical Engineering
University of Virginia
Charlottesville, VA 22908, USA
sl8jx@virginia.edu

Abu Hasnat Mohammad Rubaiyat
Department of Electrical and Computer Engineering
University of Virginia
Charlottesville, VA 22904, USA
ar3fx@virginia.edu

Gustavo K. Rohde
Department of Biomedical Engineering & Department of Electrical and Computer Engineering
Charlottesville, VA 22908, USA
gustavo@virginia.edu

ABSTRACT

Transport-based metrics and related embeddings (transforms) have recently been used to model signal classes where nonlinear structures or variations are present. In this paper, we study the geodesic properties of time series data with a generalized Wasserstein metric and the geometry related to their signed cumulative distribution transforms in the embedding space. Moreover, we show how understanding such geometric characteristics can provide added interpretability to certain time series classifiers, and be an inspiration for more robust classifiers. The appendix can be found at https://arxiv.org/abs/2206.01984.

1 INTRODUCTION

Transport-based distances, such as Wasserstein distances Villani (2003), have been shown to be an effective tool in signal analysis and machine learning applications including image retrieval Rubner et al. (2000) and registration Haker et al. (2004), modeling biological morphology Ozolek et al. (2014); Basu et al. (2014), comparing probability distributions Arjovsky et al. (2017), and providing good low-dimensional embeddings of image manifolds Hamm et al. (2022), to name a few. The success of transport-based distances are in part due to their ability to incorporate information of spatial or time deformations naturally structured in signals Kolouri et al. (2017). For example, they are observed to correctly recover biologically interpretable and statistically significant differences Basu et al. (2014) and quantify semantic differences between distributions that correlate well with human perception Rubner et al. (2000).

Within the set of problems in data science, modeling of time series data is considered a challenging problem. Deformation-based methods such as dynamic time warping Abanda et al. (2019); Lines & Bagnall (2015) have been shown successful in enabling the comparison of time series data more meaningfully. In addition to being able to align features from two different time series, Wasserstein-type distances are also true distances that can allow for a low-dimensional representation of dynamical systems in which time series can be classified and statistically analyzed Muskulus & Verduyn-Lunel (2011). In recent years, many transport transform-based techniques have been developed to leverage Wasserstein distances and linearized (L^2) embeddings to facilitate the application of many standard data analysis Kolouri et al. (2017). In particular, the cumulative distribution transform (CDT), based on the 1D Wasserstein embedding, was introduced in Park et al. (2018) as a means of classifying normalized non-negative signals, and has been extended to general signed signals via the the signed cumulative distribution transform (SCDT) in Aldroubi et al. (2022).

Wasserstein embeddings based on the cumulative distribution transform (CDT) Park et al. (2018); Rubaiyat et al. (2020); Aldroubi et al. (2022) have recently emerged as a robust, computationally

*This author is currently with the University of North Carolina, Chapel Hill (email: shiyl@unc.edu).

efficient, and accurate end-to-end classification method for time series (1D signal) classification. They are particularly effective for classifying data emanating from physical processes where signal classes can be modeled as observations of a particular set of template signals under some unknown, possibly random, temporal deformation or transportation Park et al. (2018); Shifat-E-Rabbi et al. (2021); Rubaiyat et al. (2022b). Efforts have been made to explain the success of these models by understanding the geometry of the transform embedding space Park et al. (2018); Aldroubi et al. (2021); Moosmüller & Cloninger (2020), where embedding properties and conditions when the data class becomes convex and linearly separable in the transform space are studied. In a nutshell, the template-deformation-based generative models capture the nonlinear structure of signals and the nonlinear transport transforms render signal classes that are nonlinear and non-convex into convex sets in transform embedding space (see Figure 1).

As the CDT Park et al. (2018) is defined for probability measures (or their associated density functions) which are non-negative and normalized, in this manuscript we elucidate the geometry of general time series (signed, non-normalized) with a generalized Wasserstein metric in the SCDT embedding space with a L^2-type metric. In addition to the convexity and isometric embedding properties of the SCDT Aldroubi et al. (2022), which are shared by the CDT, we look at the geodesic properties of the SCDT and illustrate the differences between geometry of data in CDT and SCDT space. In particular, the SCDT embedding $\widehat{S} \subseteq \left(L^2(s_0) \times \mathbb{R}\right)^2$ is not a geodesic space while geodesics exist between signals within a generative model (see Figure 1). As a preliminary application, we provide an interpretation of the nearest (transform) subspace classifiers proposed in Rubaiyat et al. (2022a;b) through visualizing paths between the test signals and their projections to various subspaces. In particular, we illustrate that using the training samples, these classifiers "correctly" generate a (local) subspace that models the generative clusters (see equation 9) to which the given test signals belong. We hypothesise this knowledge can lead to the design of more efficient and accurate pattern recognition tools and added interpretability of various classifiers.

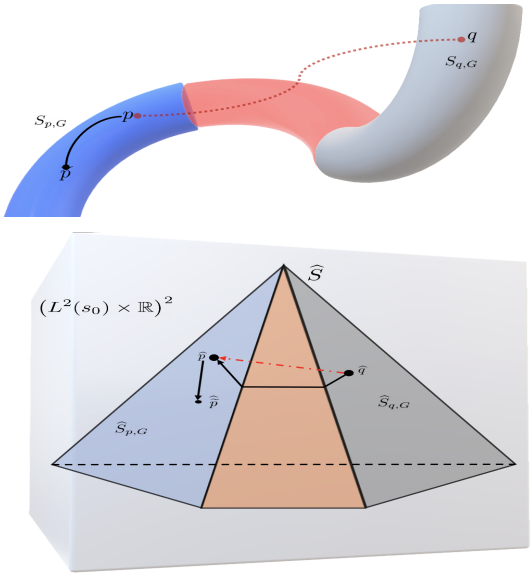

Figure 1: Space of time series with a generalized Wasserstein metric (top) and its embedding $\widehat{S}$ (bottom) are not geodesic spaces while geodesics exist between any pair of signals in the same generative cluster $S_{p,G}$. Here $\widehat{S}$ is represented as the faces of the polyhedron (see Remark 2.7 and 2.8) and its ambient space $\left(L^2(s_0) \times \mathbb{R}\right)^2$ is represented as the open cube.

Throughout the manuscript, we work with L^1 signals s with finite second moments, [1] where $\Omega_s \subseteq \mathbb{R}$ is the bounded domain over which s is defined. We denote S as the set of L^1 signals with finite second moments and S_1 as the set of non-negative L^1-normalized signals in S and $\|s\|$ as the L^1-norm of s.

[1] For bounded Ω_s, it suffices to require that $s \in L^2(\Omega_s)$, in which case by Cauchy-Schwartz $\int_{\Omega_s} t^2|s(t)|dt < \infty$; $s \in L^1(\Omega_s)$ follows from the fact that $L^2(\Omega_s) \subseteq L^1(\Omega_s)$.

2 TRANSPORT TRANSFORMS AND GEOMETRIC PROPERTIES OF TIME SERIES

We give a brief overview of the CDT and SCDT and their associated embedding properties in Section 2.1 and present the main theorems about the geodesic properties of time series with respect to a generalized Wasserstein metric and the geometry of the SCDT embedding in Section 2.2.

2.1 THE SIGNED CUMULATIVE DISTRIBUTION TRANSFORM AND A GENERALIZED WASSERSTEIN METRIC

The Cumulative Distribution Transform (CDT) was introduced in Park et al. (2018) for non-negative L^1-normalized functions. In particular, given non-negative signals s and s_0 (a fixed reference) with $\|s\| = \|s_0\| = 1$, the CDT s^* of s is defined as the optimal transport map [2] between reference s_0 and s, which is the unique non-decreasing map Santambrogio (2015)

$$s^* = F_s^\dagger \circ F_{s_0}, \tag{1}$$

where F_{s_0} is the cumulative distribution function of s_0 and $F_s^\dagger(x) := \inf\{t \in \mathbb{R} : F(t) \geq x\}$ is the generalized inverse of F_s.[3] In particular, $(s^*)_\sharp s_0 = s$ and s^* minimizes the Wasserstein-2 cost $d_{W^2}(s_0, s) := \sqrt{\inf_{s=T_\sharp s_0} \int_{\mathbb{R}} |x - T(x)|^2 s_0(x) dx}$ between s_0 and s. It is well-known Santambrogio (2015) that $\big(S_1, d_{W^2}(\cdot,\cdot)\big)$ is a geodesic space with the constant-speed geodesic between s and $\tilde{s}$ given by for $\alpha \mapsto p_\alpha = \Big((1-\alpha)id + \alpha T^*\Big)_\sharp s$, where T^* is the optimal transport map between s and $\tilde{s}$ in S_1 and $\alpha \in [0,1]$. Moreover, the CDT defines an isometric embedding from the space of non-negative normalized signals $\big(S_1, d_{W^2}\big)$ to the transform space $\big(S_1^*, L^2(s_0)\big)$ (cf. Villani (2003)), i.e.,

$$d_{W^2}(s_1, s_2) = \|s_1^* - s_2^*\|_{L^2(s_0)} \tag{2}$$

where S_1^* is the set of CDTs of signals in S_1.

Now for a (non-zero) signed signal, the Jordan decomposition Royden & Fitzpatrick (1988) is applied to $s(t) = s^+(t) - s^-(t)$,[4] where $s^+(t)$ and $s^-(t)$ are the absolute values of the positive and negative parts of the signal $s(t)$. Given a fixed L^1-normalized positive reference signal s_0 defined on Ω_{s_0}, the signed cumulative distribution transform (SCDT) Aldroubi et al. (2022) of $s(t)$ is then defined as the following tuple [5] :

$$\widehat{s} := \Big((\frac{s^+}{\|s^+\|})^*, \|s^+\|, (\frac{s^-}{\|s^-\|})^*, \|s^-\| \Big), \tag{3}$$

where $(\frac{s^\pm}{\|s^\pm\|})^*$ is the CDT (defined in eqn. (1)) of the normalized signal $\frac{s^\pm}{\|s^\pm\|}$. To simplify notations, from now on, for non-negative signals (e.g., s^+), its CDT is defined as the CDT of its normalized version, i.e., we denote $(\frac{s^+}{\|s^+\|})^*$ simply as $(s^+)^*$. Equivalently, equation 3 becomes $\widehat{s} = \big((s^+)^*, \|s^+\|, (s^-)^*, \|s^-\|\big)$. Like the CDT, the SCDT is invertible with the inverse transform (see A.5 for more details) given by [6]

$$s = \|s^+\| \Big((s^+)^*_\sharp s_0 \Big) - \|s^-\| \Big((s^-)^*_\sharp s_0 \Big). \tag{5}$$

[2] The fact that s_0 and s have finite second moments guarantees the existence of a unique optimal transport map between them.

[3] If F_s is strictly increasing on Ω_s then $F_s^\dagger = F_s^{-1}$.

[4] Here $s^+(t)$ and $s^-(t)$ can be seen as the density functions of corresponding measures in the Jordan decomposition of the measure μ_s associated with s where $d\mu_s(x) := s(x)dx$.

[5] When $s = 0$, the CDT s^* is defined to be 0 and the SCDT $\widehat{s} := (0, 0, 0, 0)$.

[6] Here $(s^\pm)^*_\sharp s_0$ denote the push-forward signal of s_0 by the maps $(s^\pm)^*$ respectively. In particular, when the maps $(s^\pm)^*$ are differentiable, the inverse formula becomes

$$\begin{aligned} s(t) =& \|s^+\| \Big((s^+)^{*^{-1}} \Big)'(t) s_0 \Big((s^+)^{*^{-1}}(t) \Big) \\ & - \|s^-\| \Big((s^-)^{*^{-1}} \Big)'(t) s_0 \Big((s^-)^{*^{-1}}(t) \Big). \end{aligned} \tag{4}$$

Similarly, a generalized Wasserstein-2 distance between two time series can be defined as follows:

$$D_S(s_1, s_2) := \left(d^2_{W^2}\Big(\frac{s_1^+}{\|s_1^+\|}, \frac{s_2^+}{\|s_2^+\|}\Big) + d^2_{W^2}\Big(\frac{s_1^-}{\|s_1^-\|}, \frac{s_2^-}{\|s_2^-\|}\Big) + \Big(\|s_1^+\| - \|s_2^+\|\Big)^2 + \Big(\|s_1^-\| - \|s_2^-\|\Big)^2 \right)^{\frac{1}{2}} \tag{6}$$

$$= \left(\|(s_1^+)^* - (s_2^+)^*\|^2_{L^2(s_0)} + \|(s_1^-)^* - (s_2^-)^*\|^2_{L^2(s_0)} + \Big(\|s_1^+\| - \|s_2^+\|\Big)^2 + \Big(\|s_1^-\| - \|s_2^-\|\Big)^2 \right)^{\frac{1}{2}}$$

$$= \|\widehat{s}_1 - \widehat{s}_2\|_{L^2(s_0)\times\mathbb{R}\times L^2(s_0)\times\mathbb{R}}, \tag{7}$$

where the second-to-last equality follows from the embedding property equation 2 of the CDT. Hence the SCDT also defines an isometry (embedding) from the space $\big(S, D_S(\cdot,\cdot)\big)$ of time series to its transform space $\Big(\widehat{S}, \|\cdot\|_{(L^2(s_0)\times\mathbb{R})^2}\Big)$.

2.2 Geodesic Properties

We first present a sufficient condition on a pair of signals under which a geodesic exists between them.

Theorem 2.1. *Fix a reference signal $s_0 \in S_1$. Given a signal $s \in S$ and a strictly increasing differentiable function $g : \mathbb{R} \to \mathbb{R}$, there is a constant speed geodesic between s and $\widetilde{s} := g's \circ g$. In particular, the geodesic $\alpha \mapsto p_\alpha$ is given by $\forall \alpha \in [0, 1]$,*

$$\begin{aligned} p_\alpha = &\big[(1-\alpha)\|s^+\| + \alpha\|\widetilde{s}^+\|\big]\Big((1-\alpha)(s^+)^* + \alpha(\widetilde{s}^+)^*\Big)_\sharp s_0 \\ &-\big[(1-\alpha)\|s^-\| + \alpha\|\widetilde{s}^-\|\big]\Big((1-\alpha)(s^-)^* + \alpha(\widetilde{s}^-)^*\Big)_\sharp s_0. \end{aligned} \tag{8}$$

Note that $p_0 = s$ and $p_1 = \widetilde{s}$.

Proof. It suffices to show that given $\alpha_1, \alpha_2 \in [0, 1]$, $D_S(p_{\alpha_1}, p_{\alpha_2}) = |\alpha_1 - \alpha_2| D_S(s, \widetilde{s})$. By the composition property of the CDT (see A.4), $(\widetilde{s}^\pm)^* = g^{-1} \circ (s^\pm)^*$. Hence we have that

$$(1-\alpha)(s^\pm)^* + \alpha(\widetilde{s}^\pm)^* = \Big((1-\alpha)id + \alpha g^{-1}\Big) \circ (s^\pm)^*.$$

Since $(1-\alpha)id + \alpha g^{-1}$ is strictly increasing and $(s^+)^*_\sharp s_0 \perp (s^-)^*_\sharp s_0$ (see A.5), it follows that $\Big((1-\alpha)(s^+)^* + \alpha(\widetilde{s}^+)^*\Big)_\sharp s_0 \perp \Big((1-\alpha)(s^-)^* + \alpha(\widetilde{s}^-)^*\Big)_\sharp s_0$ (cf. Lemma 5.4 in Aldroubi et al. (2022)). By the inverse formula in Proposition A.3, it is not hard to see that the expression in equation 8 is the Jordan decomposition of p_α, i.e., $p_\alpha^\pm = \big[(1-\alpha)\|s^\pm\| + \alpha\|\widetilde{s}^\pm\|\big]\Big((1-\alpha)(s^\pm)^* + \alpha(\widetilde{s}^\pm)^*\Big)_\sharp s_0$. Hence

$$\begin{aligned} &D_S^2(p_{\alpha_1}, p_{\alpha_2}) = D_S^2(p^+_{\alpha_1}, p^+_{\alpha_2}) + D_S^2(p^-_{\alpha_1}, p^-_{\alpha_2}) \\ =&\|(p^+_{\alpha_1})^* - (p^+_{\alpha_2})^*\|^2_{L^2(s_0)} + \|(p^-_{\alpha_1})^* - (p^-_{\alpha_2})^*\|^2_{L^2(s_0)} + \big(\|p^+_{\alpha_1}\| - \|p^+_{\alpha_2}\|\big)^2 + \big(\|p^-_{\alpha_1}\| - \|p^-_{\alpha_2}\|\big)^2 \\ =&|\alpha_1 - \alpha_2|^2\Big(\|(s^+)^* - (\widetilde{s}^+)^*\|^2_{L^2(s_0)} + \|(s^-)^* - (\widetilde{s}^-)^*\|^2_{L^2(s_0)} + \big(\|s^+\| - \|\widetilde{s}^+\|\big)^2 + \big(\|s^-\| - \|\widetilde{s}^-\|\big)^2\Big) \\ =&|\alpha_1 - \alpha_2|^2 D_S^2(s, \widetilde{s}), \end{aligned}$$

where the second-to-last equality follows from the fact that $(p^\pm_{\alpha_i})^* = (1-\alpha_i)(s^\pm)^* + \alpha_i(\widetilde{s}^\pm)^*, i = 1, 2$ (see A.5 for more details). □

Remark 2.2. The same conclusion holds if $\widetilde{s} := \lambda g's \circ g$ for any constant $\lambda > 0$ and g strictly increasing and differentiable.

Corollary 2.3. *Let $G = \{g : \mathbb{R} \to \mathbb{R} : g$ is strictly increasing and differentiable$\}$ and $p \in S$. Consider the following template-deformation based generative model Park et al. (2018)*

$$S_{p,G} := \{p_g = g'p \circ g : g \in G\}. \tag{9}$$

Then for any two signals in $S_{p,G}$, a unique constant-speed geodesic exists with respect to the generalized Wasserstein-2 metric defined in equation 6.

Proof. Let $p_i = g_i' p \circ g_i \in S_{p,G}, i = 1, 2$. It follows that $p_2 = (g_1^{-1} \circ g_2)' p_1 \circ (g_1^{-1} \circ g_2)$. Since $g_1^{-1} \circ g_2$ is also strictly increasing, by Theorem 2.1, there exists a constant speed geodesic between p_1 and p_2. □

Remark 2.4. More generally, one can show the existence of geodesics between pairs of signals in any subset U of S such that $\widehat{U}$ is convex, the proof of which is presented in **??**. By the convexity property of the SCDT Aldroubi et al. (2022), $\widehat{S}_{p,G}$ is convex if and only if G^{-1} is convex. Hence Corollary 2.3 can be seen as a special case of Proposition A.1 since the set $G = G^{-1}$ is convex for $G = \{g : \mathbb{R} \to \mathbb{R} : g \text{ is strictly increasing and differentiable}\}$.

Next we show that a geodesic may not exist between arbitrary two signals in S with the generalized Wasserstein metric.

Theorem 2.5. *The metric space* $\big(S, D_S(\cdot, \cdot)\big)$ *is not a geodesic space.*

Proof. Recall that a metric space is geodesic means that for any two given elements, there exists a path between such that the length of the path equals the distance between them. We prove this theorem by giving an example where the length of any path between some $s_1, s_2 \in S$ is larger than their distance $D_S(s_1, s_2)$. Let $s_1 = \mathbb{1}_{[-1,0)} - \mathbb{1}_{[0,1]}$ and $s_2 = \mathbb{1}_{[0,1]} - \mathbb{1}_{[-1,0)}$.[7] Assume by contradiction that there is a path $\gamma : [0, 1] \to S$ where $\gamma_0 = s_1$ and $\gamma_1 = s_2$ such that $\text{Len}(\gamma) = D_S(s_1, s_2)$. By the embedding property equation 7 of the SCDT, it follows that $\widehat{\gamma}_\alpha(\alpha \in [0, 1])$ defines a geodesic in $\widehat{S} \subseteq (L^2(s_0) \times \mathbb{R})^2$. Since the space $(L^2(s_0) \times \mathbb{R})^2$ is uniquely geodesic (see A.6), then $\widehat{\gamma}_\alpha = (1-\alpha)\widehat{s}_1 + \alpha\widehat{s}_2$. Let $\widehat{s}_1 = (f_1^+, 1, f_1^-, 1) \in \widehat{S}$ and it is not hard to see that $\widehat{s}_2 = (f_1^-, 1, f_1^+, 1)$. Hence $\widehat{\gamma}_{1/2} := (f_{1/2}^+, a, f_{1/2}^-, b) = (\frac{f_1^+ + f_1^-}{2}, 1, \frac{f_1^+ + f_1^-}{2}, 1)$, which is a contradiction to the fact that $\widehat{\gamma}_{1/2} \in \widehat{S}$ (since by definition $(f_{1/2}^+)_\sharp s_0$ and $(f_{1/2}^-)_\sharp s_0$ should be mutually singular, see A.5). □

Remark 2.6. Using the fact that the space $(L^2(s_0) \times \mathbb{R})^2$ is uniquely geodesic, one can show that if the geodesic in $\big(S, D_S(\cdot, \cdot)\big)$ exists between two signals s and $\widetilde{s}$, it should be of the form equation 8.

Remark 2.7. Observing from Proposition A.1, it is not hard to see that $\widehat{S}$ is not convex. This is in contrast to the fact the embedding CDT space S_1^* is convex Aldroubi et al. (2021).

Remark 2.8. The set G in Corollary 2.3 is a group with the group operation being composition and defines an equivalence relation in S via $s \sim \widetilde{s}$ if and only if $\widetilde{s} = g's \circ g$ for some $g \in G$. It follows that S can be partitioned into disjoint clusters $\bigcup_i S_{p_i,G}$ (see equation 9). Hence by Remark 2.4 $\widehat{S}$ can be partitioned as a union of convex subsets $\bigcup_i \widehat{S}_{p_i,G}$.

2.3 Examples of Geodesics

In this section, we give two examples (Figure 2) where a unique geodesic exists between the given signals and two examples (Figure 3) where a geodesic does not exist. By Remark 2.6, the geodesic p_α for $\alpha \in [0, 1]$ is of the form equation 8 when it exists. In the case when a geodesic does not exist, we plot a path in S according to equation 8. For a geodesic p_α with $p_0 = s$ and $p_1 = \widetilde{s}$, it follows by definition that $\sum_{i=1}^n D_S(p_{\alpha_{i-1}}, p_{\alpha_i}) = D_S(s, \tilde{s})$ for $0 = \alpha_0 < \alpha_1 < \cdots < \alpha_n = 1$; while $\sum_{i=1}^n D_S(p_{\alpha_{i-1}}, p_{\alpha_i}) > D_S(s, \tilde{s})$ if $\alpha \mapsto p_\alpha, \alpha \in [0, 1]$ is not a geodesic path. In particular, in the following plots the signals p_{α_i} where $\alpha_i = \frac{i}{4}, i = 0, \cdots, 4$ are presented and distances $D_i := D_S(p_{\alpha_{i-1}}, p_{\alpha_i}), i = 1, 2, 3, 4$ and $D := D_S(s, \tilde{s})$ are shown.

3 A Preliminary Application : Interpreting the SCDT Subspace Classifier

In this section, we attempt to utilize the preliminary geodesic properties discussed above to partially interpret the decisions made by the SCDT subspace classifiers proposed in Rubaiyat et al. (2022b) and Rubaiyat et al. (2022a), which were shown to achieve very high accuracy in classifying segmented time series events.

[7] Here $\mathbb{1}_{[a,b]}$ denotes the indicator function of interval $[a, b]$.

[8] By a direct computation (see A.8), we have that the geodesic is given by $p_\alpha(t) = s(\frac{1}{\alpha}t)$ for $\alpha \in (0, 1]$ and $p_0 := 0$.

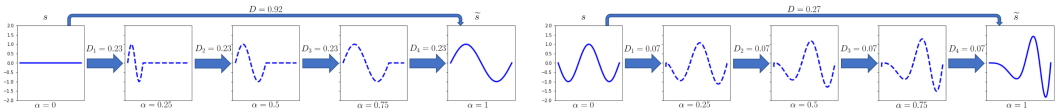

Figure 2: Examples of geodesics: (left) the geodesic between the zero signal and $s(t) = \sin(2\pi t)\mathbb{1}_{[0,1]}(t)$ where $p_\alpha(t) = \sin\big(2\pi\frac{1}{\alpha}t\big)\mathbb{1}_{[0,\alpha]}(t)$.[8] (right) the geodesic between $s(t) = -\sin(3\pi t)\mathbb{1}_{[0,1]}(t)$ and $\widetilde{s} = g's \circ g$ where $g(t) = t^2$. In both examples, $D = \sum_{i=1}^{4} D_i$.

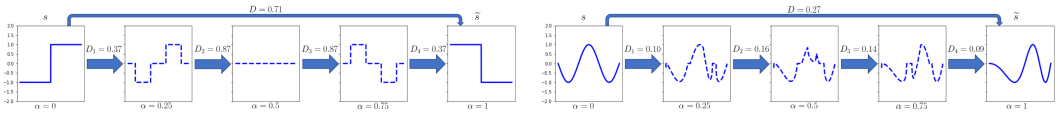

Figure 3: Examples where geodesics do not exist: (left) signal path p_α defined by equation 8 between $s = -\mathbb{1}_{[0,.5]} + \mathbb{1}_{(.5,1]}$ and $\widetilde{s} = \mathbb{1}_{[0,.5]} - \mathbb{1}_{(.5,1]}$; for this path $D = .71 \ll \sum_{i=1}^{4} D_i = 2.48$. (right) signal path p_α defined by equation 8 between s and $\widetilde{s} = s \circ g$ where $g(t) = t^2$ and $s(t) = -\sin(3\pi t)\mathbb{1}_{[0,1]}(t)$. Note the $\widetilde{s}$ here differs from that in second example of Figure 2 (there is no normalizing term $g'(t)$ here); for path $D = .27 \ll \sum_{i=1}^{4} D_i = .49$.

3.1 SCDT SUBSPACE CLASSIFIERS

The signed cumulative distribution transform (SCDT) combined with a subspace classifier has recently been shown very effective in classifying time series data Rubaiyat et al. (2022b;a). In Rubaiyat et al. (2022b), the authors employed a nearest subspace search technique in SCDT space to classify time series events that follow a certain generative model: $S^{(c)} = \{s_j^{(c)} | s_j^{(c)} = g_j' \varphi^{(c)} \circ g_j, g_j \in G^{(c)}, g_j' > 0\}$, where $s_j^{(c)}$ a signal in class c deformed from $\varphi^{(c)}$ (a template pattern corresponding to class c), and $G^{(c)}$ denotes a set of increasing deformations of a specific kind (e.g. translation, scaling, etc.). In the embedding (transform) space, each signal class is hypothesized to be modeled well by the containing subspace $\widehat{V}^{(c)} = \text{span}\big(\widehat{S}^{(c)}\big)$, and the corresponding classifier searches for the nearest subspace to the test sample to predict its class label.

An extension of the SCDT nearest subspace approach was proposed in Rubaiyat et al. (2022a), where a more general multi-template generative model was used, assuming that a signal class is generated from a set of templates under some unknown deformations. Formally, the multi-template generative model for signal class c is defined to be the set: $S^{(c)} = \bigcup_{m=1}^{M_c} S_{\varphi_m^{(c)}, G_m^{(c)}}$, where $S_{\varphi_m^{(c)}, G_m^{(c)}} = \left\{ s_{j,m}^{(c)} | s_{j,m}^{(c)} = g_j' \varphi_m^{(c)} \circ g_j, g_j' > 0, g_j \in G_m^{(c)} \right\}$ and $\left(G_m^{(c)}\right)^{-1} = \left\{ \sum_{i=1}^{k} \alpha_i f_{i,m}^{(c)}, \alpha_i \geq 0 \right\}$ lies in a linear space of deformations. Each signal class is hypothesized to be modeled well by a union of subspaces $\bigcup_{m=1}^{M_c} \widehat{V}_m^{(c)}$ in the embedding (transform) space, where $\widehat{V}_m^{(c)} = \text{span}\big(\widehat{S}_{\varphi_m^{(c)}, G_m^{(c)}}\big)$. The corresponding classifier searches for the nearest local subspace $\widehat{V}_{m*}^{(c)}$ to the test sample to predict the class label.

3.2 INTERPRETATION OF THE SCDT SUBSPACE CLASSIFIERS

As explained in the section above, the SCDT subspace classifiers search for the nearest subspace $\widehat{V}^{(c)}$ Rubaiyat et al. (2022b) or local subspace $\widehat{V}_{m*}^{(c)}$ Rubaiyat et al. (2022a) to a given test signal in SCDT (embedding) space. In particular, for the nearest subspace classifier, it can be shown that under certain assumptions, $d^2(\widehat{s}, \widehat{V}^{(c)}) < d^2(\widehat{s}, \widehat{V}^{(p)})$ for $s \in S^{(c)}$ and $p \neq c$, where $d^2(\cdot, \cdot)$ denotes the L^2-metric. Similar properties hold for the nearest local subspace classifier. The class labels are then predicted by searching for the (local) subspace with the smallest distance to the test signal.

In this paper, we provide a preliminary interpretation of the subspace classifiers using a synthetic dataset and a real dataset *StarLightCurves* Rebbapragada et al. (2009) hosted by the UCR time series classification archive Dau et al. (2018). In particular, we present a visualization of the paths between a test signal and its projections onto the subspaces associated with different classes. The projection $\widetilde{s}$ of a test signal s onto the subspace $\widehat{V}^{(c)}$ associated with class c is defined in the sense that $\widehat{\widetilde{s}} := P_{\widehat{V}^{(c)}}\widehat{s}$, where $P_{\widehat{V}^{(c)}}$ denotes the L^2-projection operator to the subspace $\widehat{V}^{(c)}$.

If the classifier can successfully model a subspace (using training data) that contains a test signal s, then the projection $\widetilde{s} = s$. In practice, we observe that the path defined by equation 8 between a test signal s and its projection $\widetilde{s}$ to a subspace associated with the same class as s consists of signals of similar shapes (or looks like a geodesic lying in the same class) and $s \approx \widetilde{s}$. On the other hand, the path between s and its projection to a subspace associated with a different class seems to exhibit unpredictable behavior.

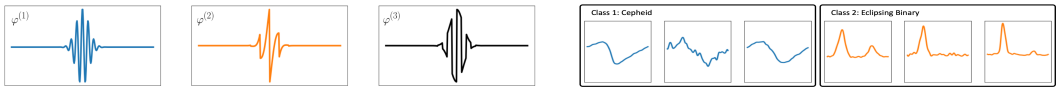

(a) Three prototype (template) signals used to generate synthetic data in Experiment 1.

(b) Samples from two classes in the *StarLightCurves* dataset.

Figure 4

Experiment 1: For this experiment, we created a synthetic dataset of three classes consisting of scaled and translated signals of three template signals: Gabor wave, apodized sawtooth wave, and apodized square wave, respectively (shown in Figure 4a). The training samples were generated following the generative model given by: $S^{(c)} = \{g'\varphi^{(c)} \circ g | g \in G\}$, where $G = \{g = \omega t + \tau, \omega > 0, \tau \in \mathbb{R}\}$ and $\varphi^{(c)}(t)$ denotes the template corresponding to class c (see Figure 4a). Here the test sample (not present in training set) follows the generative model for class 1 (Gabor wave). The signal paths p_α between the test signal and its projections onto three subspaces formed via the subspace classifier Rubaiyat et al. (2022b) are shown in Figure 5. We observe that the projection onto class 1 resembles the test signal and the corresponding path looks like a geodesic (i.e., the ratio $\sum_{i=1}^{4} D_i/D \approx 1$), indicating the subspace $\widehat{V}^{(1)}$ generated by the subspace classifier contains the SCDTs of the test signal s and its cluster $S_{s,G}$ [9]. However the paths from the test signal to its projections onto the other two classes contain signals that belong to neither classes and seem to exhibit unpredicted patterns.

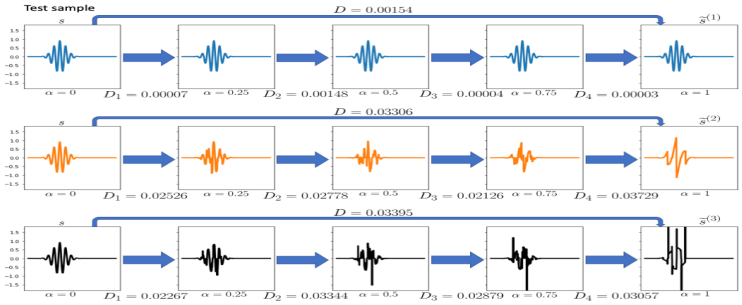

Figure 5: Signal path p_α defined by eq. (8) between a test sample s from class 1 and its projections $\tilde{s}^{(1)}, \tilde{s}^{(2)}, \tilde{s}^{(3)}$ associated with the subspaces obtained by the subspace classifier Rubaiyat et al. (2022b) corresponding to the three classes, respectively. Note that the distance D between s and $\widetilde{s}^{(1)}$ (i.e., $D_S(s, \widetilde{s}^{(1)})$) is the smallest, and hence the classifier predicts the correct label.

Experiment 2: We conducted a similar experiment with a real dataset *StarLghtCurves* Rebbapragada et al. (2009), where two classes: 'Cepheid' (class 1) and 'Eclipsing Binary' (class 2) were used. Sample signals from these two classes are shown in Figure 4b. Signal paths p_α are presented in Figure

[9] Since the same phenomenon is observed for any random test signal following the generative model $S_{\varphi^{(1)},G}$, which equals $S_{s,G}$ for an arbitrary signal s in class 1 since G is the set of affine deformations.

6 from a test signal s_j in each class ($j = 1, 2$) to their projections $\widetilde{s}_j^{(i)}$ corresponding to subspaces $\widehat{V}^{(i)}$ ($i = 1, 2$) produced by the local subspace classifier proposed in Rubaiyat et al. (2022a). We observe that the path from s_j to its projection $\widetilde{s}_j^{(j)}$ associated with the same class resembles a geodesic within class j (see the first and the fourth row in Figure 6) while the path from s_j to its projection $\widetilde{s}_j^{(i)}$ associated with a different class $i \neq j$ contains very noisy signals which seem to belong to neither classes (see the second and third row of Figure 6).

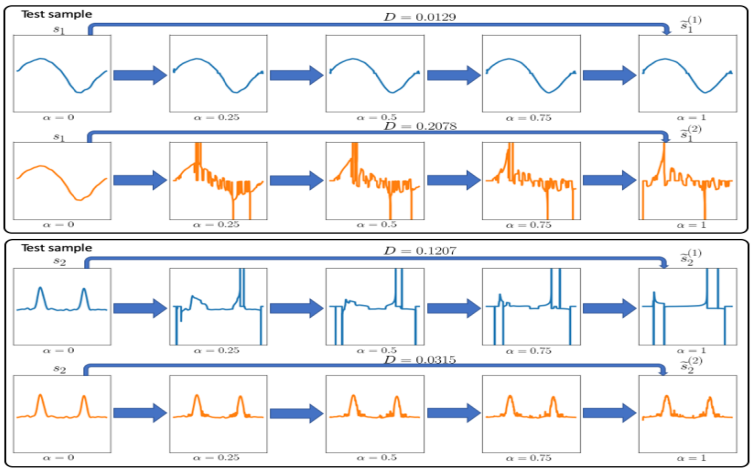

Figure 6: Signal path p_α defined by eq. (8) between a test sample s_j and its projections $\tilde{s}_j^{(i)}$ ($i, j = 1, 2$) in the local subspaces obtained by the subspace classifier Rubaiyat et al. (2022a) corresponding to two classes, respectively. Note that in the top panel the distance D between s_1 and $\widetilde{s}_1^{(1)}$ (i.e., $D_S(s_1, \widetilde{s}_1^{(1)})$) is smaller, and in the bottom panel the distance D between s_2 and $\widetilde{s}_2^{(2)}$ is smaller. Hence the local classifier predicts the correct labels in both cases.

Remark 3.1. Given the stark differences between the path from a signal to its projection associated with a subspace of its own class and that to its projection associated with a subspace of a different class, one may consider using the length of the path (see e.g., $\sum_i D_i$ in Figure 5) as the classification metric, in contrast to the D_S distance between the signal and its projection used in the aforementioned subspace classifiers, which we leave to future work.

4 Conclusion

In this preliminary study, we look into the geometry of time series with respect to a generalized Wasserstein metric and its embedding in a linear space. In particular, a geodesic may not exist between two arbitrary time series in S but exists between signals within the same generative cluster (see equation 9). We utilize this knowledge to show whether the (local) subspaces formed by the training samples via the SCDT subspace classifiers do a good job in modeling the signal classes conforming to certain generative modeling assumptions. We illustrate it by visualizing the paths between random test signals and their projections onto the corresponding subspaces associated with different classes and observe that there is a path resembling a geodesic from a test signal to its projection in the subspace associated with the same class of the test signal. This shows some preliminary evidence that the classifiers produce a "good" subspace that models the corresponding generative clusters to which the test signals belong. In the future, we are interested in quantitative (numerical) characterization of geodesics for real/noisy data in the hope of building more robust models and classifiers for time series events.

5 Acknowledgments

This work was supported in part by NIH grants GM130825, GM090033.

REFERENCES

A. Abanda, U. Mori, and J. A Lozano. A review on distance based time series classification. *Data Mining and Knowledge Discovery*, 33(2):378–412, 2019.

A. Aldroubi, S. Li, and G. K. Rohde. Partitioning signal classes using transport transforms for data analysis and machine learning. *Sampling Theory, Signal Processing, and Data Analysis*, 19(1): 1–25, 2021.

A. Aldroubi, R. D. Martin, I. Medri, G. K. Rohde, and S. Thareja. The signed cumulative distribution transform for 1-D signal analysis and classification. *Foundations of Data Science*, 2022.

M. Arjovsky, S. Chintala, and L. Bottou. Wasserstein generative adversarial networks. In *International conference on machine learning*, pp. 214–223. PMLR, 2017.

S. Basu, S. Kolouri, and G. K. Rohde. Detecting and visualizing cell phenotype differences from microscopy images using transport-based morphometry. *Proceedings of the National Academy of Sciences*, 111(9):3448–3453, 2014.

H. A. Dau, E. Keogh, K. Kamgar, C. M. Yeh, Y. Zhu, S. Gharghabi, C. A. Ratanamahatana, Y. Chen, B. Hu, N. Begum, A. Bagnall, A. Mueen, G. Batista, and Hexagon-ML. The UCR time series classification archive, October 2018. `https://www.cs.ucr.edu/~eamonn/time_series_data_2018/`.

S. Haker, L. Zhu, A. Tannenbaum, and S. Angenent. Optimal mass transport for registration and warping. *International Journal of computer vision*, 60(3):225–240, 2004.

K. Hamm, N. Henscheid, and S. Kang. Wassmap: Wasserstein isometric mapping for image manifold learning. *arXiv preprint arXiv:2204.06645*, 2022.

S. Kolouri, S. R. Park, M. Thorpe, D. Slepcev, and G. K Rohde. Optimal mass transport: Signal processing and machine-learning applications. *IEEE signal processing magazine*, 34(4):43–59, 2017.

J. Lines and A. Bagnall. Time series classification with ensembles of elastic distance measures. *Data Mining and Knowledge Discovery*, 29(3):565–592, 2015.

C. Moosmüller and . Cloninger, A. Linear optimal transport embedding: Provable wasserstein classification for certain rigid transformations and perturbations. *arXiv preprint arXiv:2008.09165*, 2020.

M. Muskulus and S. Verduyn-Lunel. Wasserstein distances in the analysis of time series and dynamical systems. *Physica D: Nonlinear Phenomena*, 240(1):45–58, 2011.

J.A. Ozolek, A. B. Tosun, W. Wang, C. Chen, S. Kolouri, S. Basu, H. Huang, and G. K. Rohde. Accurate diagnosis of thyroid follicular lesions from nuclear morphology using supervised learning. *Medical image analysis*, 18(5):772–780, 2014.

S. R. Park, S. Kolouri, S. Kundu, and G. K. Rohde. The cumulative distribution transform and linear pattern recognition. *Applied and computational harmonic analysis*, 45:616–641, 2018.

U. Rebbapragada, P. Protopapas, C.E Brodley, and C. Alcock. Finding anomalous periodic time series. *Machine learning*, 74(3):281–313, 2009.

H. L. Royden and P. Fitzpatrick. *Real analysis*, volume 32. Macmillan New York, 1988.

A. H. M. Rubaiyat, K. M. Hallam, J. M. Nichols, M. N. Hutchinson, S. Li, and G. K. Rohde. Parametric signal estimation using the cumulative distribution transform. *IEEE Transactions on Signal Processing*, 68:3312–3324, 2020.

A.H.M. Rubaiyat, S. Li, X. Yin, M. Shifat-E-Rabbi, Y. Zhuang, and G. K Rohde. End-to-end signal classification in signed cumulative distribution transform space. *arXiv preprint arXiv:2205.00348*, 2022a.

A.H.M Rubaiyat, M. Shifat-E-Rabbi, Y. Zhuang, S. Li, and G. K. Rohde. Nearest subspace search in the signed cumulative distribution transform space for 1d signal classification. In *ICASSP 2022-2022 IEEE International Conference on Acoustics, Speech and Signal Processing (ICASSP)*, pp. 3508–3512. IEEE, 2022b.

Y. Rubner, C. Tomasi, and L. J. Guibas. The earth mover's distance as a metric for image retrieval. *International journal of computer vision*, 40(2):99–121, 2000.

F. Santambrogio. Optimal transport for applied mathematicians. *Birkäuser, NY*, 55(58-63):94, 2015.

M. Shifat-E-Rabbi, X. Yin, A. H. M. Rubaiyat, S. Li, S. Kolouri, A. Aldroubi, J. M. Nichols, and G. K. Rohde. Radon cumulative distribution transform subspace modeling for image classification. *Journal of Mathematical Imaging and Vision*, pp. 1–19, 2021.

C. Villani. *Topics in Optimal Transportation*. Number 58. American Mathematical Soc., 2003.